Supplementary Information

Structural insights into the mechanism of the human SGLT2–MAP17 glucose transporter

Masahiro Hiraizumi[1,4,†,*], Tomoya Akashi[2,4], Kouta Murasaki[1], Hiroyuki Kishida[1], Taichi Kumanomidou[1], Nao Torimoto[1], Osamu Nureki[3,*], and Ikuko Miyaguchi[1,*]

[1]Discovery Technology Laboratories Sohyaku Innovative Research Division, Mitsubishi Tanabe Pharma Co., LTD., 1000, Kamoshida cho, Aoba ku, Yokohama 227 0033, Japan
[2]DMPK Research Laboratories Sohyaku Innovative Research Division, Mitsubishi Tanabe Pharma Co., LTD., 1000, Kamoshida-cho, Aoba-ku, Yokohama 227-0033, Japan
[3]Department of Biological Sciences, Graduate School of Science, The University of Tokyo, 7-3-1 Hongo, Bunkyo-ku, Tokyo 113-0033, Japan
[4]Co-first authors
[*]Corresponding authors
[†]Current address: Department of Chemistry and Biotechnology, Graduate School of Engineering, The University of Tokyo

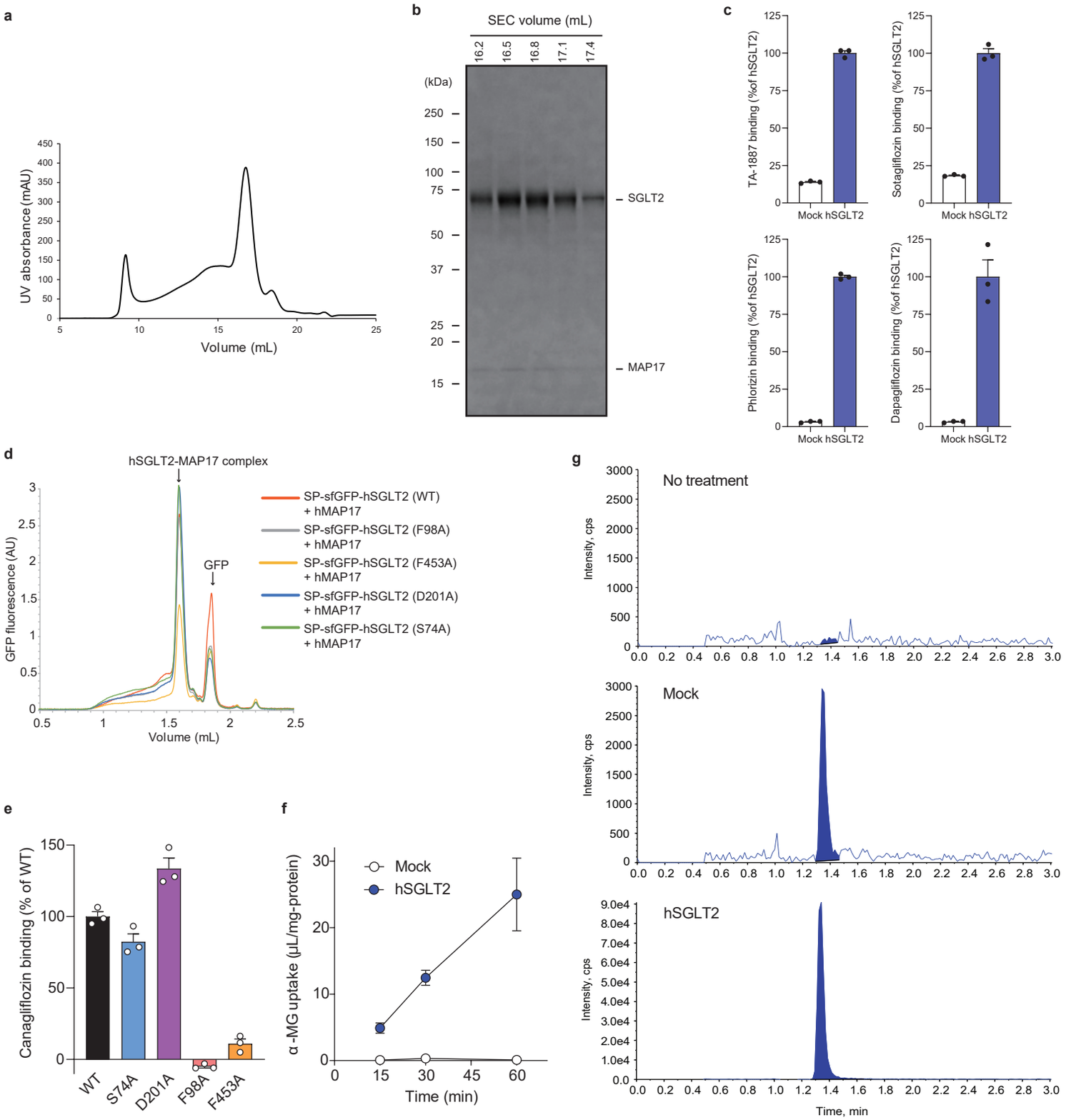

Supplementary Figure 1. Biochemical characterization of the hSGLT2–MAP17 complex.

(a) Representative size-exclusion chromatography profile of hSGLT2–MAP17. (b) SDS-PAGE analysis of the hSGLT2–MAP17 peak fractions via size-exclusion chromatography (SEC) purification. (c) SGLT2 inhibitors (25 nM) binding to the crude membrane expressing hSGLT2 and MAP17 (n = 3, technical replicates). (d) FSEC profiles for various mutations of sfGFP-tagged hSGLT2 with MAP17. The arrows indicate the elution positions of the hSGLT2–MAP17 heterodimer and the free GFP (GFP). (e) Canagliflozin binding to the crude membrane expressing wild-type hSGLT2 and mutants. Crude membranes were incubated with 30 nM canagliflozin and binding was measured by LC-MS/MS. Data are shown as mean ± SEM (n = 3, technical replicates). (f) Time-course of hSGLT2-mediated α-MG uptake. α-MG uptake (500 μM) by hSGLT2-expressing cells and mock cells was examined. Each point represents mean ± SEM (n = 4, biological replicates). (g) Chromatograms of α-MG in the lysates of untreated mock cells (No treatment), mock cells incubated with α-MG (Mock), and hSGLT2- and MAP17-expressing cells incubated with α-MG (hSGLT2).

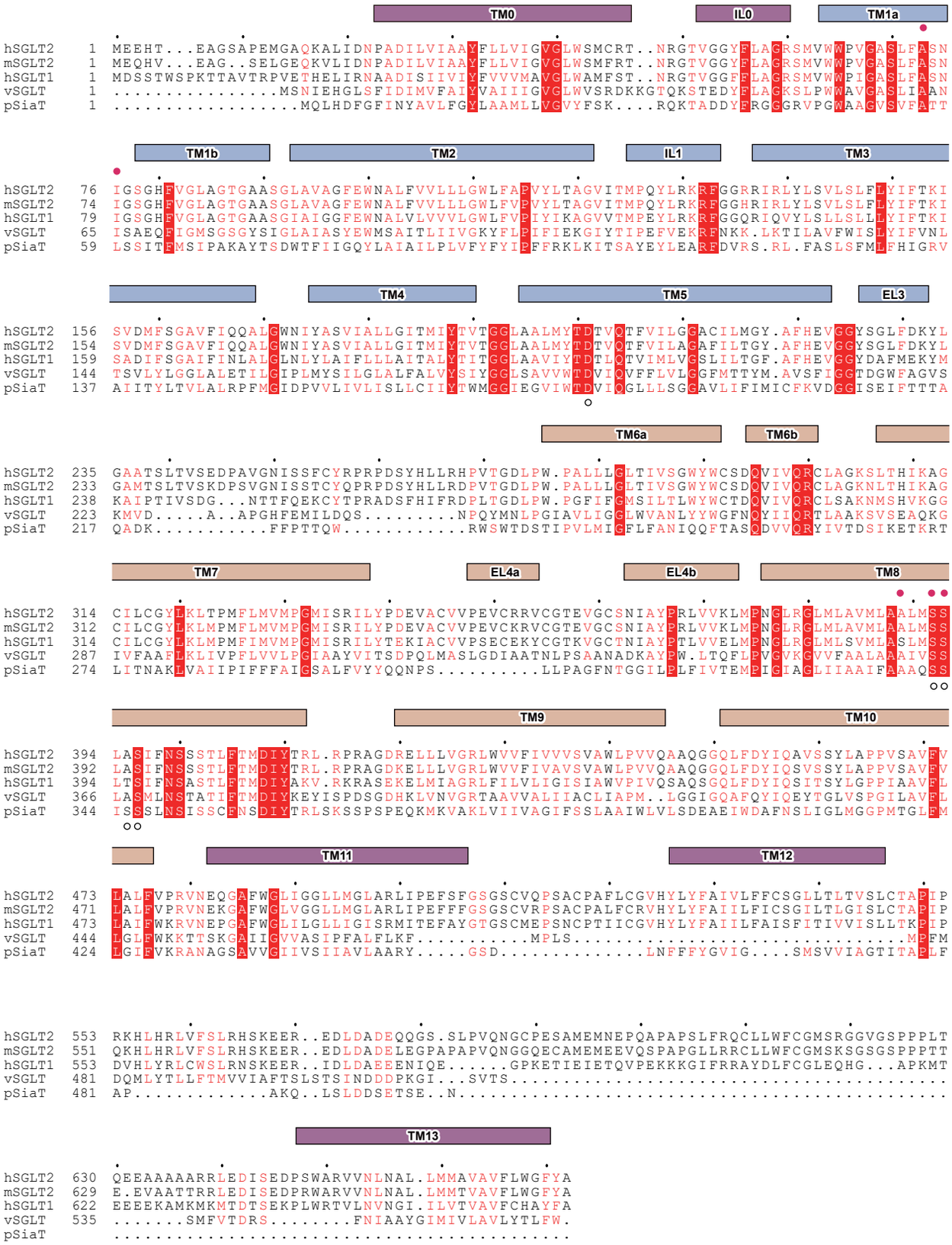

Supplementary Figure 2. Sequence alignment of SGLT.

Sequence alignment of hSGLT2 (UniProt: P31639), mSGLT2 (UniProt: Q92317), hSGLT1 (UniProt: P13866), Vibrio parahaemolyticus SGLT (UniProt: P96169), and Proteus mirabilis HI4320 sialic acid symporter (UniProt: B4EZY7), performed using Clustal Omega. Conserved transmembrane helices of hSGLT2 are indicated above the sequences. The similarly conserved residues are indicated by red letters. The residues at the conserved Na2 and Na3 sites of SGLT are highlighted with pink circles above or white circles below the alignment, respectively.

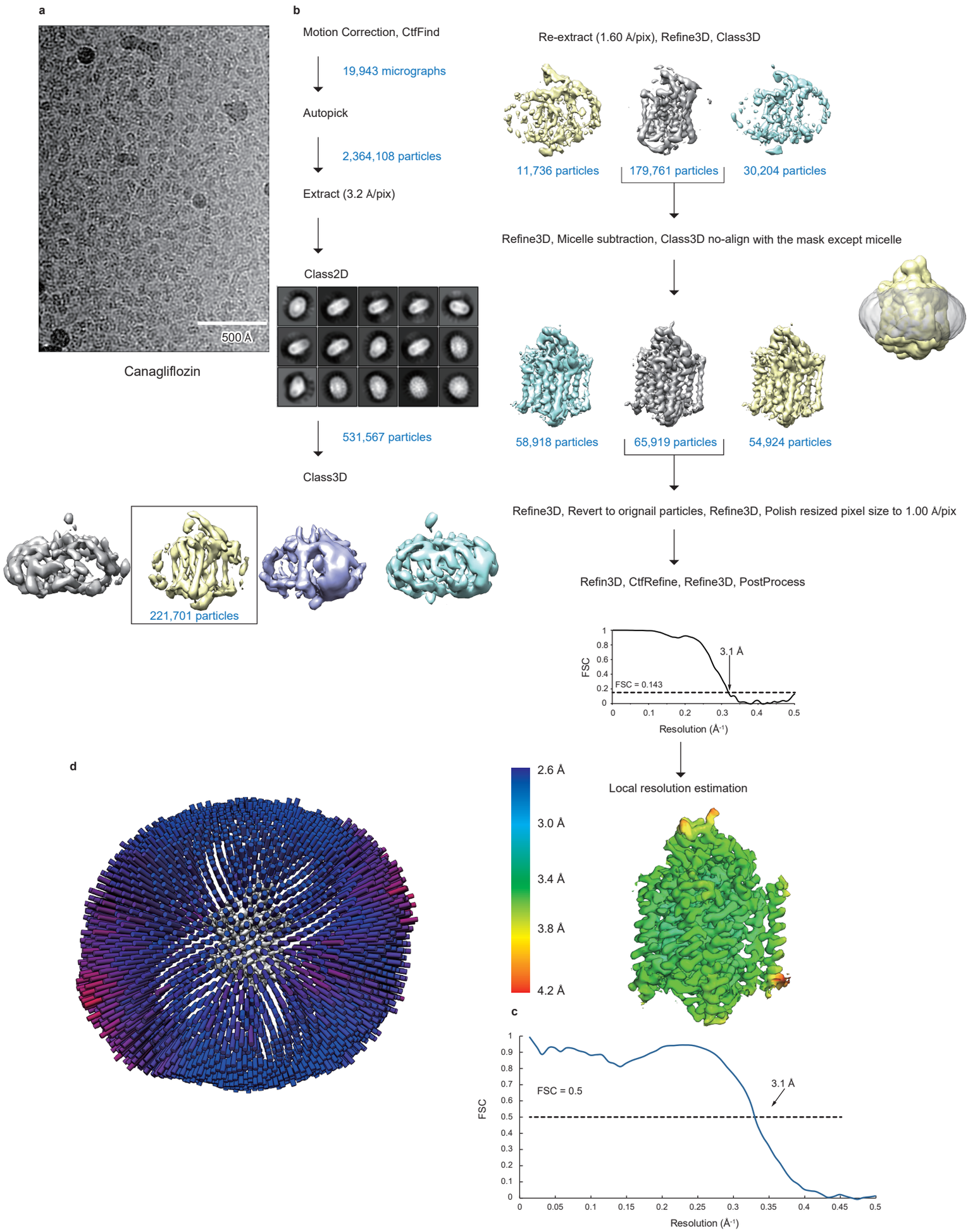

Supplementary Figure 3. Data processing of the canagliflozin-bound state.

(a) Representative cryo-EM image of the hSGLT2–MAP17 complex in the presence of canagliflozin. (b) Data processing workflow of single-particle image-processing and local-resolution analysis. Particles were separated into three groups via non-aligned 3D classification, with the mask (without micelles) shown in yellow. (c) Cross-validation FSC curves for map-to-model fitting. (d) Angular distributions of the final reconstruction.

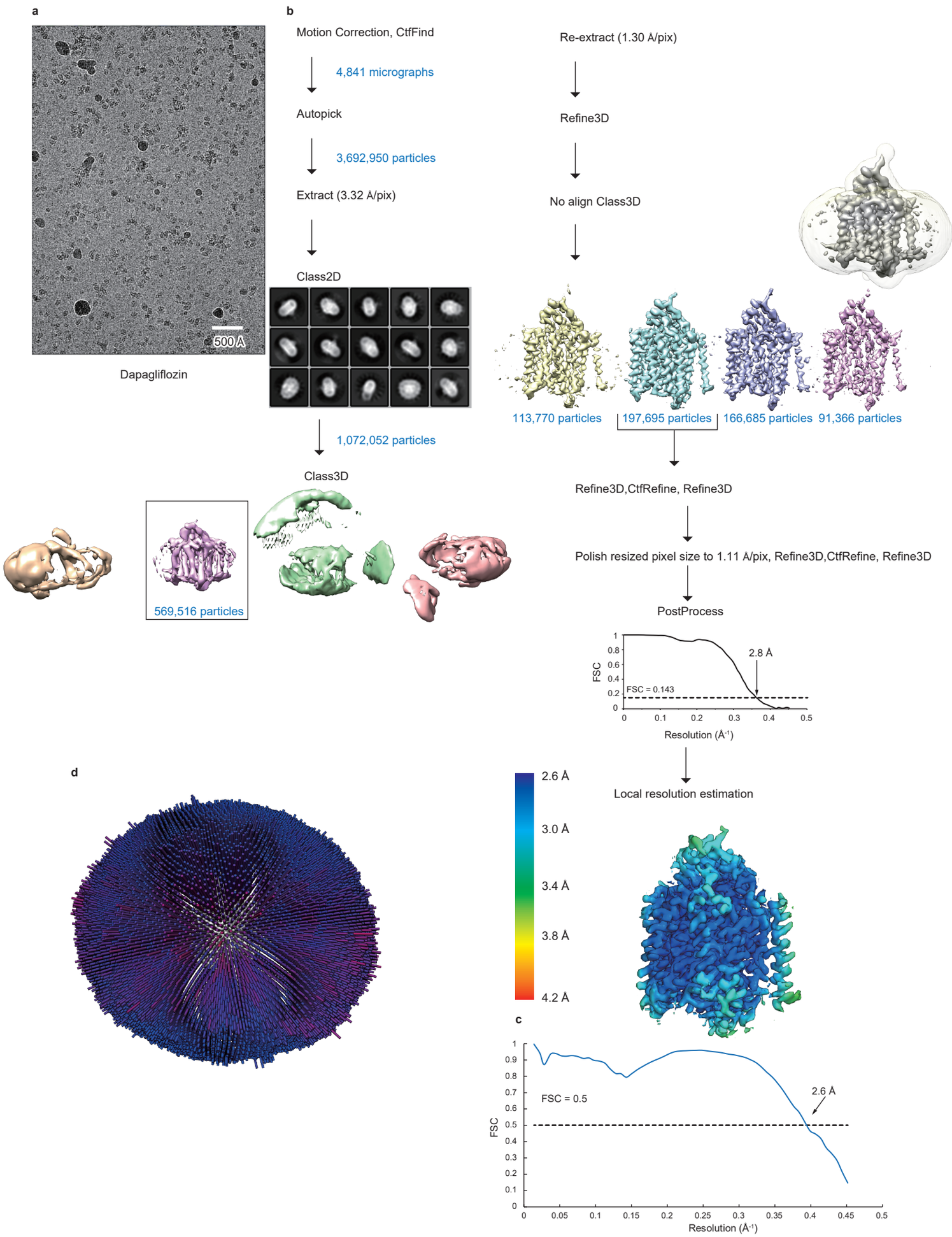

Supplementary Figure 4. Data processing of the dapagliflozin-bound state.

(a) Representative cryo-EM image of the hSGLT2–MAP17 complex in the presence of dapagliflozin. (b) Data processing workflow of single-particle image-processing and local-resolution analysis. Particles were separated into four groups by non-aligned 3D classification, with the mask (without micelles) shown in transparent white. (c) Cross-validation FSC curves for map-to-model fitting. (d) Angular distributions of the final reconstruction.

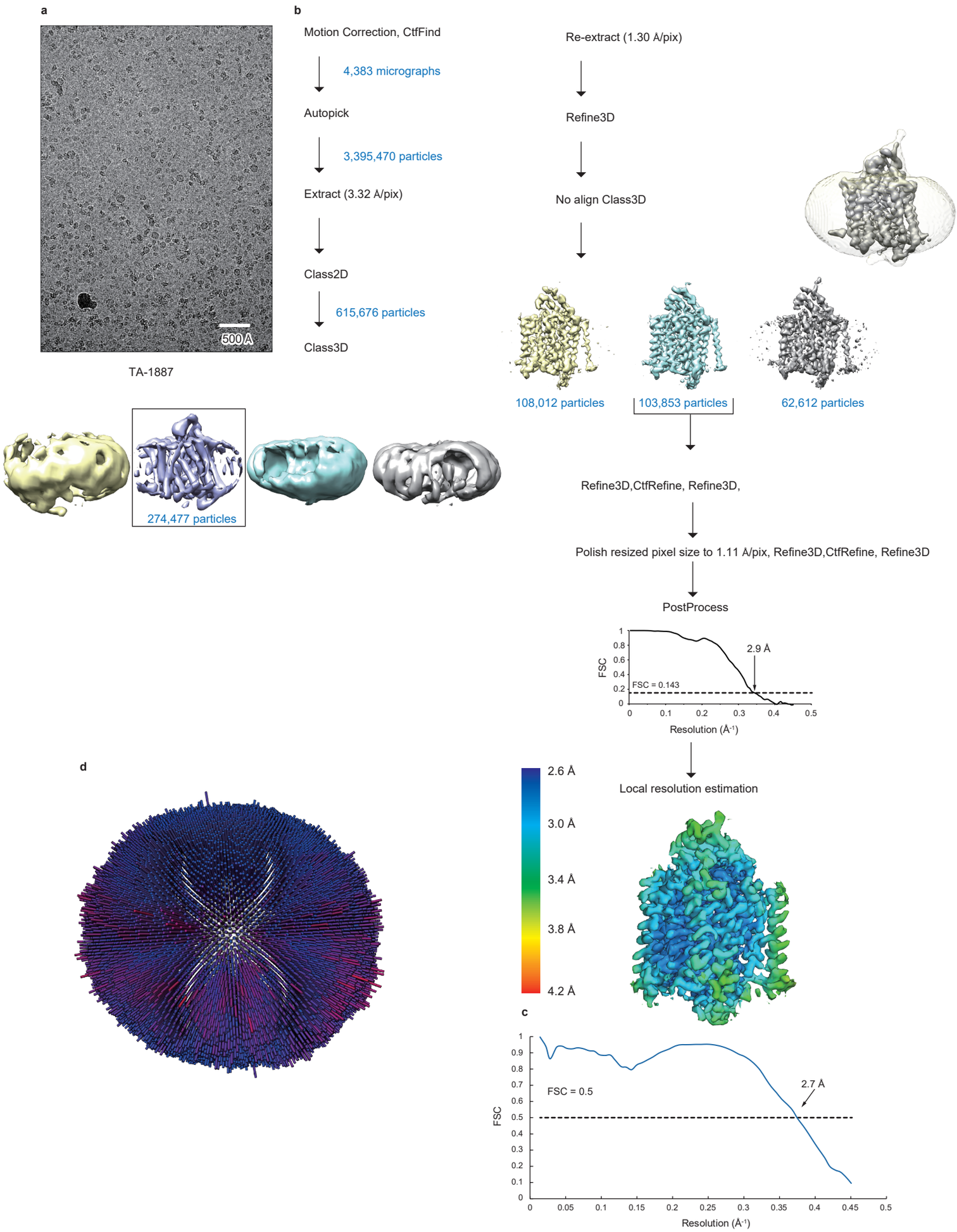

Supplementary Figure 5. Data processing of the TA-1887-bound state.

(a) Representative cryo-EM image of the hSGLT2–MAP17 complex in the presence of TA-1887. (b) Data processing workflow of single-particle image-processing and local-resolution analysis. Particles were separated into three groups via non-align 3D classification, with the mask covering the proteins and micelle shown in transparent white. (c) Cross-validation FSC curves for map-to-model fitting. (d) Angular distributions of the final reconstruction.

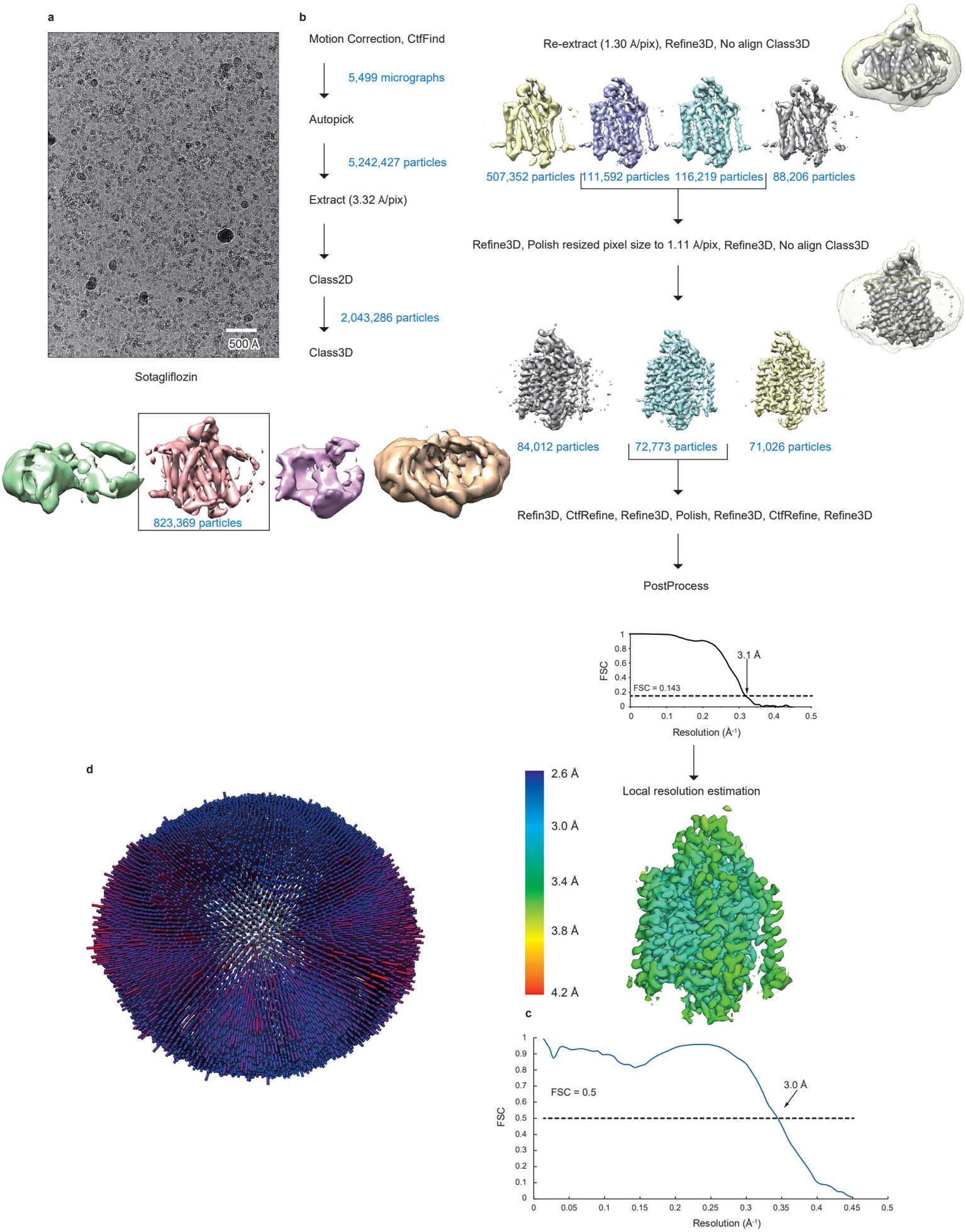

Supplementary Figure 6. Data processing of the sotagliflozin-bound state.

(a) Representative cryo-EM image of the hSGLT2–MAP17 complex in the presence of sotagliflozin. (b) Data processing workflow of single-particle image-processing and local-resolution analysis. Particles were separated into three groups via two rounds of non-aligned 3D classification, with the mask covering the proteins and micelles shown in transparent white. (c) Cross-validation FSC curves for map-to-model fitting. (d) Angular distributions of the final reconstruction.

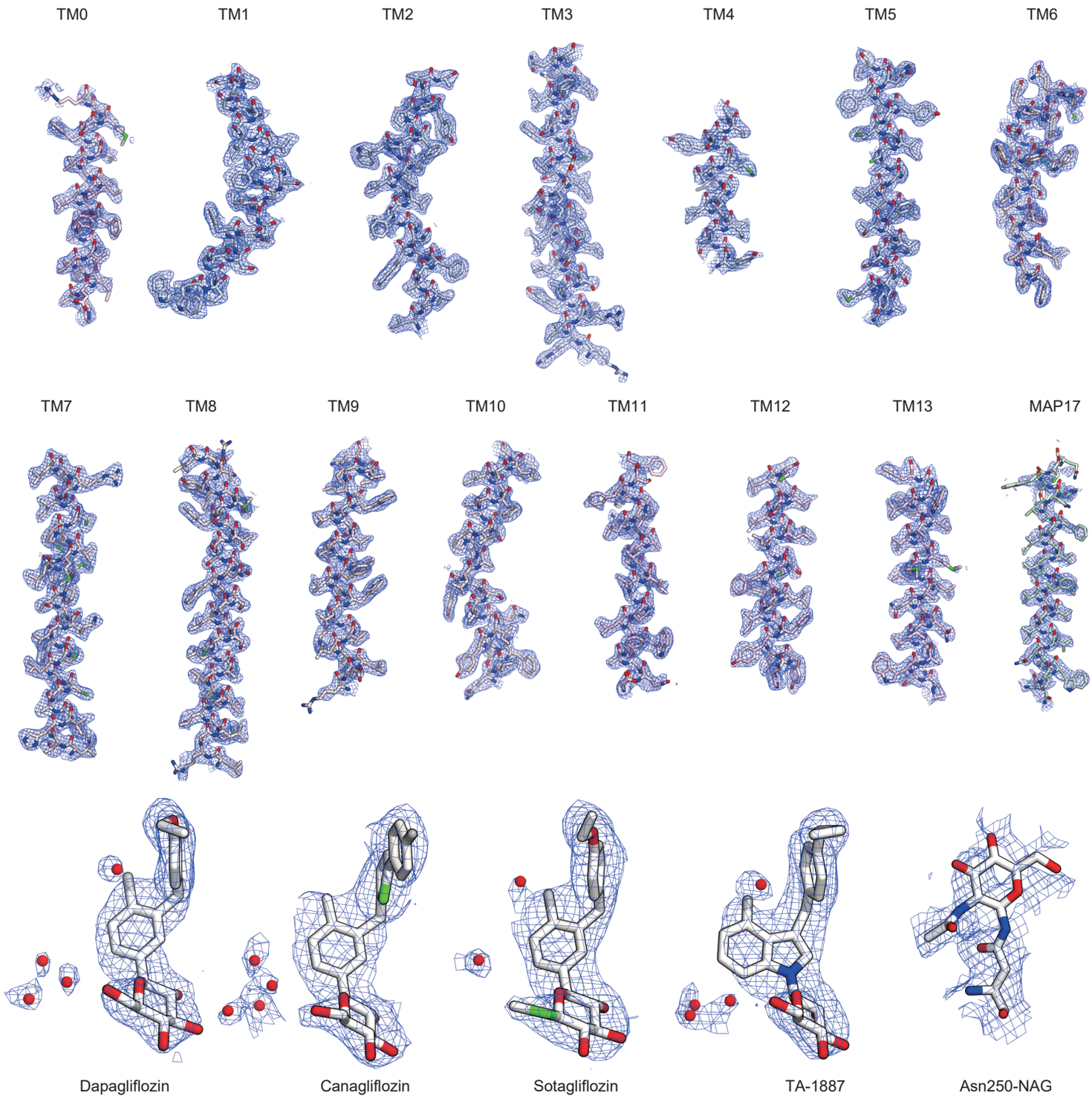

Supplementary Figure 7. The outward-opening model of hSGLT2–MAP17 in the density maps.

The cryo-EM density and atomic model of each segment of the outward-opening model hSGLT2–MAP17, inhibitors, and glycosylation sites, contoured to 3.0 σ, 4.0 σ, and 2.0 σ, respectively. Red spheres: water molecules around the inhibitors.

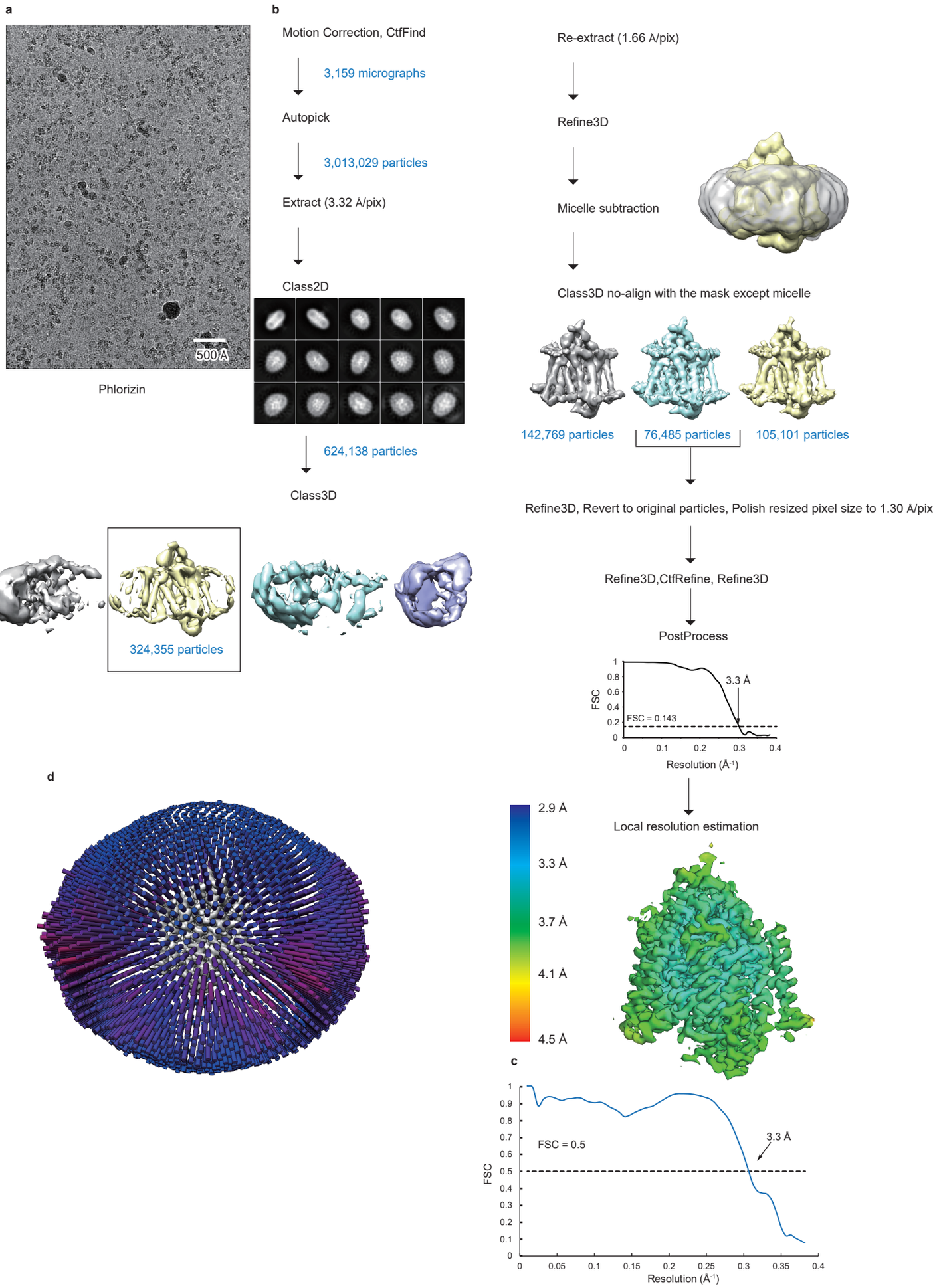

Supplementary Figure 8. Data processing of the phlorizin-bound state.

(a) Representative cryo-EM image of the hSGLT2–MAP17 complex in the presence of phlorizin. (b) Data processing workflow of single-particle image-processing and local-resolution analysis. Particles were separated into three groups by non-aligned 3D classification, with the mask covering the proteins (without micelles) shown in yellow. (c) Cross-validation FSC curves for map-to-model fitting. (d) Angular distributions of the final reconstruction.

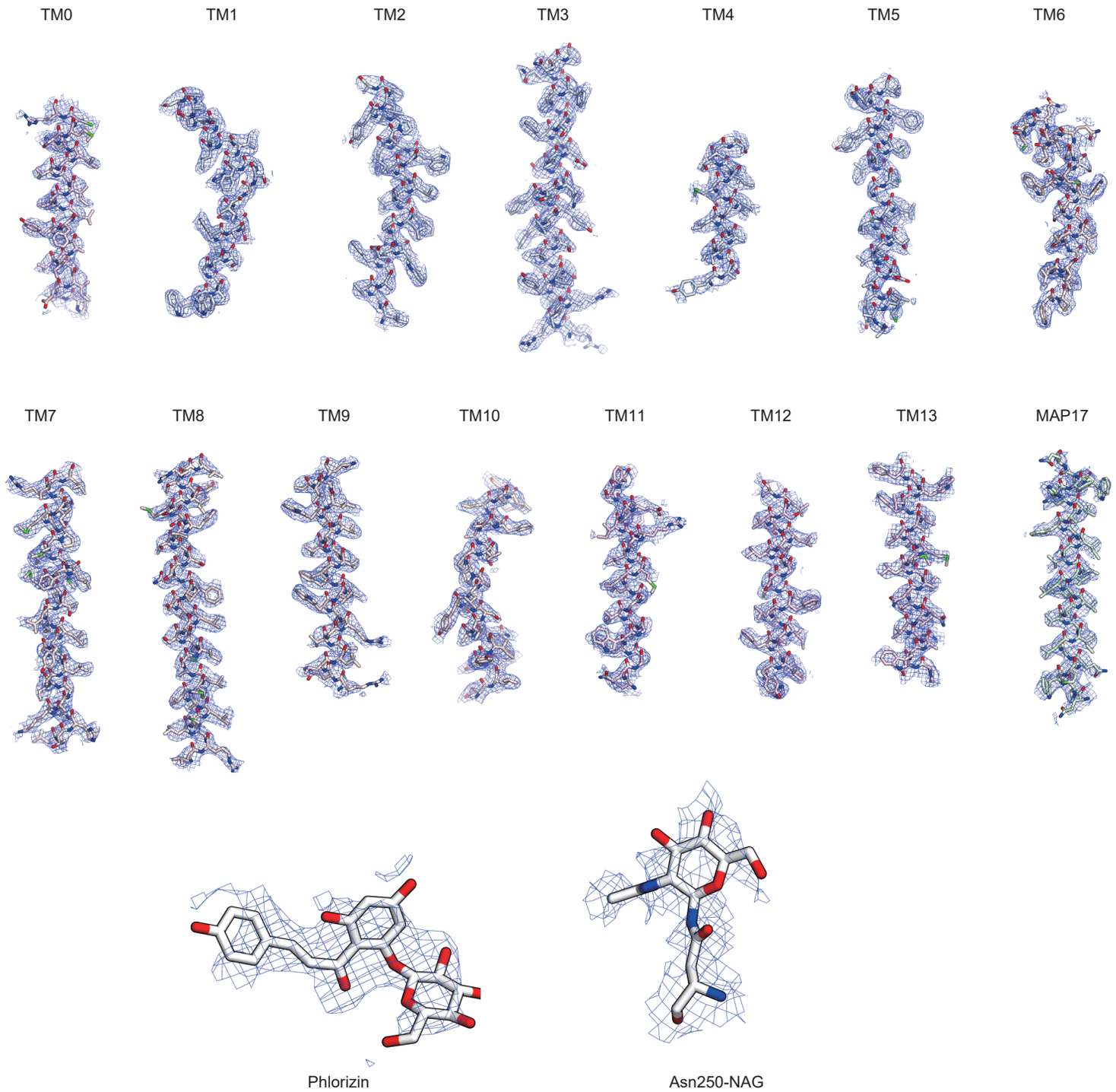

Supplementary Figure 9. Inward-open model of hSGLT2–MAP17 in the density maps.

The cryo-EM density and atomic models of each segment of the inward-open model of hSGLT2–MAP17, phlorizin, and glycosylation sites, contoured to 2.9 σ, 2.7 σ, and 2.7 σ, respectively.

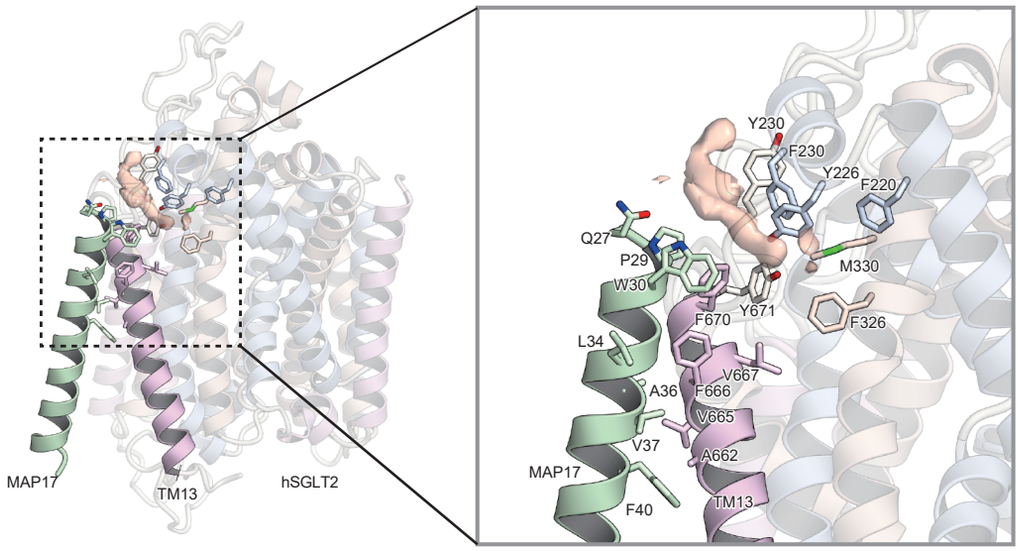

Supplementary Figure 10. MAP17 and SGLT2 interaction site.

The density of the lipid molecule (orange) is observed between MAP17 and SGLT2.

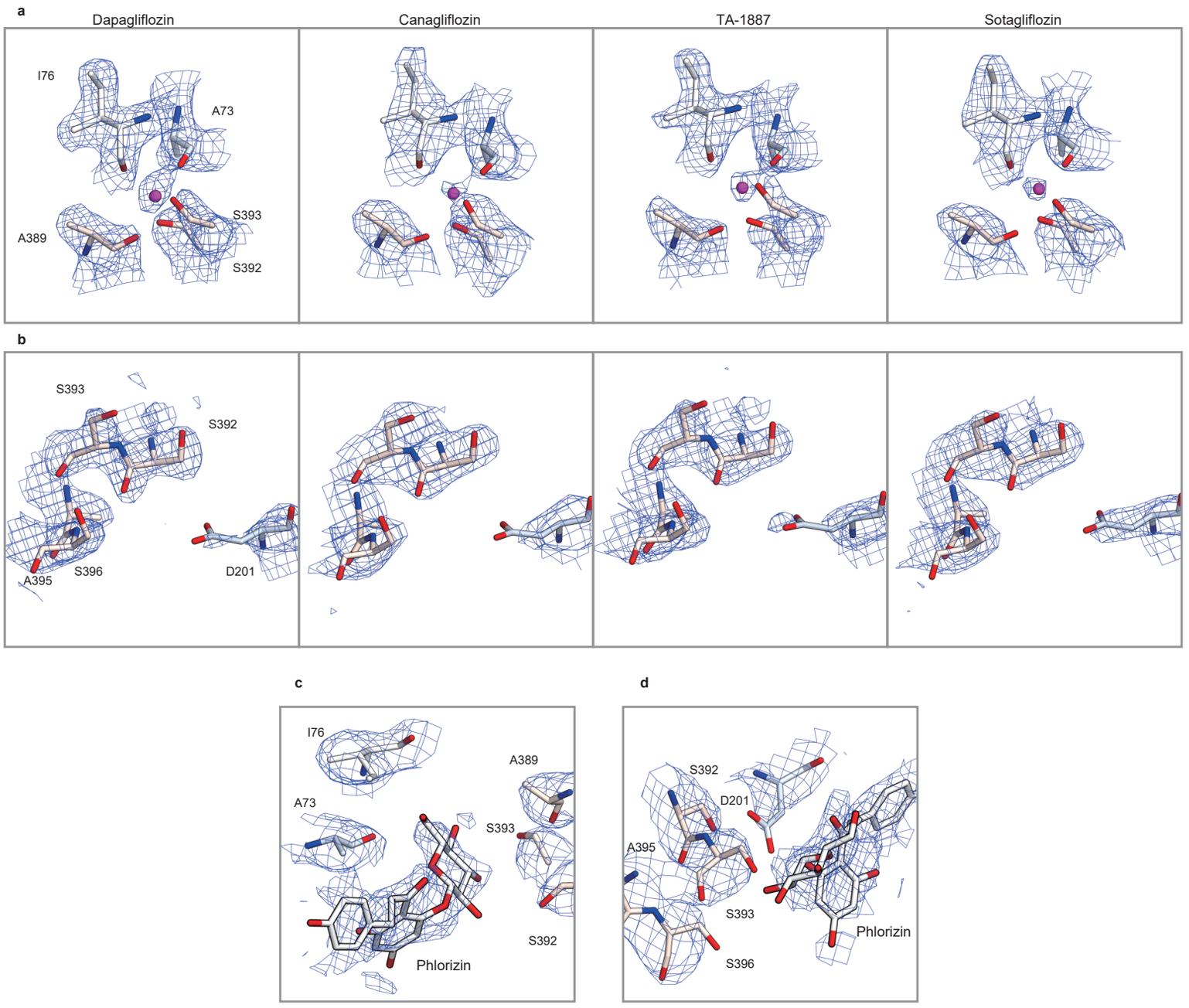

Supplementary Figure 11. Sodium ion-binding sites of SGLT2

(a) The sodium ion-binding Na2 sites of dapagliflozin, canagliflozin, TA-1887, and sotagliflozin are shown. (b) Sites in SGLT2 corresponding to Na3 sites where the other sodium ion binds in SGLT1. No electron density corresponding to a sodium ion can be observed. (c, d) The sodium ion-binding Na2 sites, and the sites corresponding to Na3 sites of the phlorizin-bound inward-open conformation. The phlorizin binding site is near the Na2 and Na3 sites.

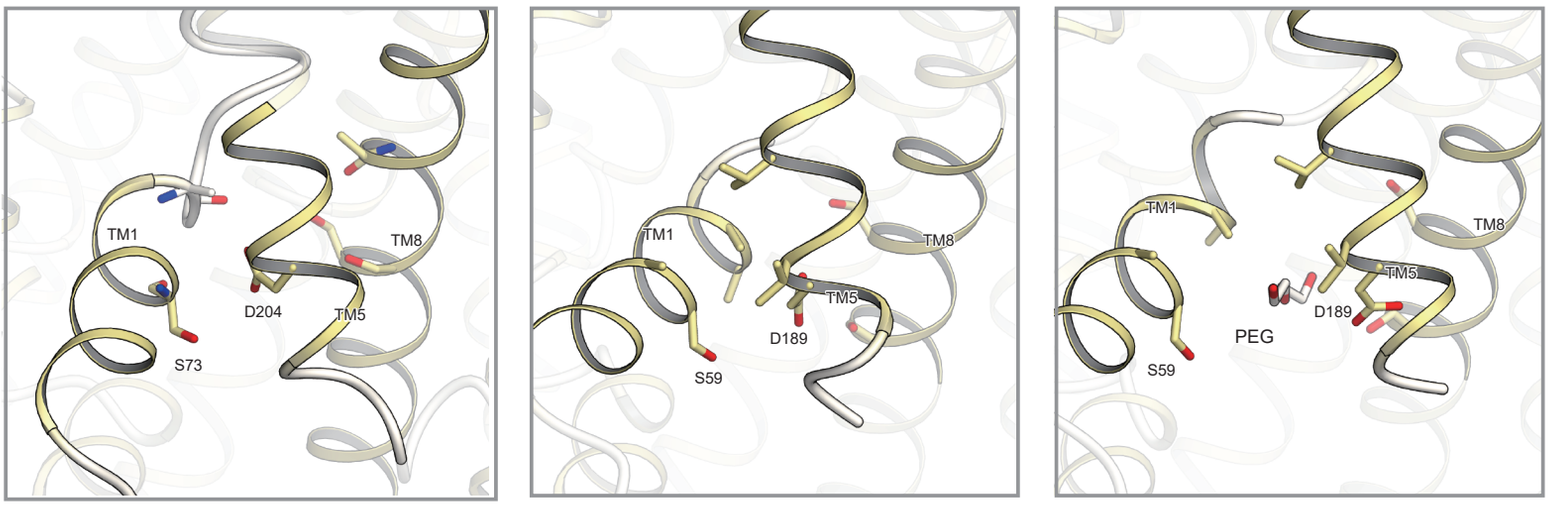

hSGLT1 (PDB : 7sla)

vSGLT (PDB : 3dh4)

vSGLT (PDB : 2xq2)

Supplementary Figure 12. Comparison of the inward conformation of other SGLT structures.

Structural comparison of sites corresponding to the intracellular phlorizin-binding sites of SGLT2. From left to right, inward-occluded conformation of hSGLT1, inward-occluded conformation of vSGLT, and inward-open conformation of vSGLT. The structures are viewed from the membrane side.

Supplementary Data Table 1.

Data collection, processing, model refinement, and validation. Clash scores, rotamer outliers, and Ramachandran plots were calculated using the Servalcat pipeline.

Data collection and processing					
State	Outward	Outward	Outward	Outward	Inward
EMDB-ID	EMD-34673	EMD-34705	EMD-34610	EMD-34737	EMD-34823
PDB ID	8HDH	8HEZ	8HB0	8HG7	8HIN
Inhibitor	Canagliflozin	Dapagliflozin	TA-1887	Sotagliflozin	Phlorizin
Microscope	Titan Krios G4	Titan Krios G3i			
Detector	Gatan K3 Camera with Quantum LS energy filter				
Magnification	215,000	105,000			
Voltage (kV)	300				
Electron exposure (e^{-}/Å^2)	64				
Defocus range (μm)	-0.6 to -1.6	-0.8 to -1.6			
Pixel size (Å/px)	0.4	0.83			
Symmetry imposed	C1				
Number of movies	19,943	4,841	4,383	5,499	3,159
Initial particle images	2,364,108	3,692,950	3,395,470	5,242,427	3,013,029
Final particle images	65,919	197,695	103,853	72,773	76,485
Map resolution (Å)	3.1	2.8	2.9	3.1	3.3
FSC threshold	0.143	0.143	0.143	0.143	0.143
Map sharpening B factor (Å^2)	-107.9	-95.4	-75.8	-96.4	-144.5
Model building and refinement					
Model composition					
Protein atoms	4,728	4,692	4728	4,763	4,743
Metals	1	1	1	1	0
Other atoms	49	46	49	44	45
R.M.S. deviations from ideal					
Bond lengths (Å)	0.011	0.012	0.012	0.015	0.018
Bond angles (°)	1.876	1.859	1.943	2.010	2.368
Validation					
Clashscore	5.62	6.29	6.66	6.72	10.28
Rotamer outliers (%)	1.20	2.22	1.20	2.39	4.58
Ramachandran plot					
Favored (%)	95.9	97.4	95.7	96.1	92.9
Allowed (%)	4.1	2.6	4.3	3.9	7.1
Outlier (%)	0.0	0.0	0.0	0.0	0.0

Supplementary Data Table 2.

Kinetic parameters of canagliflozin binding in the membrane fraction of hSGLT2-expressing and MAP17-expressing cells, in the presence or absence of Na^+.

	Na(+)	Na(-)
B_{max}	99.9 ± 8.5	69.3 ± 6.2
K_d	94.0 ± 21.7	109 ± 25.4

Data were represented in mean ± SEM (n = 3, technical replicates)

Supplementary Data Table 3.

Kinetic parameters of phlorizin and phloretin binding in the membrane fraction of wild-type cells or cells expressing mutated hSGLT2 and MAP17.

	Phlorizin			
Construct	K_{d1} (nM)	B_{max1} (pmol/mg-protein)	K_{d2} (nM)	B_{max2} (pmol/mg-protein)
WT	28.1 ± 11.3	0.356 ± 0.069	12400 ± 6900	16.8 ± 7.4
S74A	113 ± 16	1.16 ± 0.07	ND	ND
D201	72.2 ± 10.0	0.550 ± 0.028	ND	ND
F98A	ND	ND	ND	ND
F453A	ND	ND	ND	ND

	Phloretin	
Construct	K_d (nM)	B_{max} (pmol/mg-protein)
WT	12000 ± 1900	51.7 ± 3.46
S74A	ND	ND
D201	ND	ND

Data were represented in mean ± SEM (n = 3, technical replicates)
ND; not determined

Supplementary Data Table 4.

IC50 values of phlorizin in α-MG uptake by wild-type and mutant hSGLT2.

Construct	IC50 (nM)
WT	57.0 ± 8.49
S74A	145 ± 27
F98A	1640 ± 1720
F453A	468 ± 200

Data were represented in mean ± SEM (n = 4, biological replicates)